American Journal of Applied Chemistry
2025, Vol. 13, No. 5, pp. 139-151
https://doi.org/10.11648/j.ajac.20251305.12

Research Article

Biosynthesis of Silver Nanoparticles Based on *Senna Alata* and Striking Dynamization of a Ternary Fe°/S/Pz Filter Device for Electrochemical Remediation of Phosphates in Water

Mintang Fongang Ulrich Armel[1], Suzanne Makota S. N.[1, *], Fran çois Eya'ane Meva[2], Ngameni Chiege Dylane Stephane[1], Djokam Dongue Serge Aime[1], Dipita Kolye Ernest Yves Herliche[1], Watat Vanessa Adrielle[1], Youna Ngueyep Armel[1], Tsegui Tabou Rubain[1], Feze Mekiedje Yves-Thierry[1]

[1]Department of Chemistry, Faculty of Sciences, University Douala, Douala, Cameroon

[2]Department of Pharmaceutical Sciences, Faculty of Medicine and Pharmaceutical Sciences, University of Douala, Douala, Cameroon

Abstract

Fe °/H_2O systems have already proven remediation properties. Though, due to the early clogging of 100% Fe °-bed devices, the site of electrochemical corrosion products (CPs), they are associated with non-expansive porous materials such as pozzolan (Pz), and natural coal (NC), in binary (Fe °/Pz, Fe °/NC), ternary (Fe °/S/Pz, Fe °/S/NC) or quaternary configurations Fe °/S/Pz/C (Iron/Sand/Pozzolan/Natural coal), thus making the thickness of the reactive zone (RZ) dependent on the proportion of materials. A ternary Fe °/S/Pz filter system with a heterogeneous RZ, embedded between two sand layers, was enhanced with a small amount of silver nanoparticle (AgNp) based on *senna alata* (*SA*). The resulting new device was studied for an operation of its nanometric size, and its very large reactive surface, since it's an herbaceous plant, 30 to 50 cm tall, of the *fabaceae* family, without characteristic flavor or smell, however with numerous antifungal, antibacterial and corrosion inhibitory properties. Eighteen (18) filtering devices were tested for this, including six (6) 100% Fe °, (6) 25% Fe °/50% S/25% Pz, and (6) 25% Fe °/48.75% S/25% Pz/1.25% Np. Phosphates, components of fertilizers and agricultural waste 0.2 g/L K_2HPO_4, at pH=5 was used as operative indicator. The experiments lasted forty (40) days per device. We measured the pH, phosphates removal rate, dissolved iron, flow rate, Conductivity and redox potential. Thus, it appears that Np *SA* in Fe °/S/Pz allow a resurgence of efficiency, such as 100% Fe° < 25% Fe°/50% S/25% Pz < 25% Fe°/48.75% S/25% Pz/1.25% Np. A rate of about 1% of the silver Np *SA* effectively contributes to the phosphate removal process, the thickness of the RZ is not changed, the pH is in line with WHO recommendations, the flow rate is acceptable. Although fluctuating, the measured conductivities and redox potentials are low for all devices, confirming the same oxidation degree of iron released.

Keywords

Aqueous Corrosion, Fe °-Bed Filters, Nanoparticles, Phosphates, Pozzolan, Sand, *Senna Alata*

*Corresponding author: s.makota@laposte.net (Suzanne Makota S. N.)

Received: 7 July 2025; **Accepted:** 28 July 2025; **Published:** 9 September 2025

1. Introduction

The physicochemical and bacteriological decontamination power of Fe °-bed filters is now acquired, due to the electrochemical process of iron (Fe °) oxidation, which generates corrosion products (CPs) that are likely to cause clogging in the long run [1-10]. Fe ° cannot coexist with water, its oxidation generates Fe^{2+} ions and precipitation products depending on the pH.

$$(1)\quad Fe \rightarrow 2e^-$$
$$(2)\quad 2H_2O \rightarrow 2H^+$$
$$(3)\quad Fe^{2+} + 2OH^- \rightarrow Fe(OH)_2$$

In an anoxic environment, the ions Fe^{2+}present can form iron (II) hydroxides $Fe(OH)_2$, which will evolve into iron (III) hydroxides $Fe(OH)_3$ and generate rust [11-18]. The more or less weakness of Fe ° in contact with water depends on pH, according to the Pourbaix diagrams $E = f(pH)$ of the superposition of water boundaries and those of Fe ° [19, 20]. Three (3) zones thus appear, including an immunity zone in which the iron is stable, a corrosion zone in which it is oxidized, the concentration of dissolved species are greater than 10^{-6} mol/L, and finally, a passivation zone corresponding to the stability of solid species, most often a metal oxide**.** The study of electrochemical formed products depending on pH allows to measure the redox potentials of the couples in presence [18], such as:

$$(4)\quad Fe^{2+}/Fe \;;\; Fe^{2+} + 2e^- \leftrightarrows Fe$$
$$E(V)\quad E(Fe^{2+}/Fe) = E°(Fe^{2+}/Fe) + \frac{0,06}{2} log[Fe^{2+}]$$
$$(5)\quad Fe^{3+}/Fe^{2+} \;;\; Fe^{3+} + 1e^- \leftrightarrows Fe^{2+}$$
$$E(V)\quad E(Fe^{3+}/Fe^{2+}) = E°(Fe^{3+}/Fe^{2+}) + 0,06log\frac{[Fe^{3+}]}{[Fe^{2+}]}$$
$$(6)\quad Fe(OH)_3/Fe^{2+} \;;\; Fe(OH)_3 + 1e^- + 3H^+ \leftrightarrows Fe^{2+} 3H_2O$$
$$E(V)\quad E(Fe(OH)_3/Fe^{2+}) = E°(Fe(OH)_3/Fe^{2+}) + 0,06log\frac{[H^+]^3}{[Fe^{2+}]}$$
$$(7)\quad Fe(OH)_3/Fe(OH)_2 \;;\; Fe(OH)_3 + 1e^- + 1H^+ \leftrightarrows Fe(OH)_2 + H_2O$$
$$E(V)\quad E(Fe(OH)_3/Fe(OH)_2) = E°(Fe(OH)_3/Fe(OH)_2) + 0,06log[H^+]$$
$$(8)\quad Fe(OH)_2/Fe \;;\; Fe(OH)_2 + 2e^- + 2H^+ \leftrightarrows Fe + 2H_2O$$
$$E(V)\quad E(Fe(OH)_2/Fe) = E°(Fe(OH)_3/Fe) + \frac{0,06}{2} log[H^+]^2$$

All these potentials are measurable thanks to the Nernst relation and constitute as many proofs of electronic transfers and the presence of the Cps of iron. However, many studies, including those of Harza [21], have shown that 100% Fe ° devices are not viable. The filters of the 3-Kolshi, Sono and KAF generation have also increased their limits, either because of their short lifespan or because of their low efficiency in the removal of micropollutants, microorganisms, and viruses. Indeed, the 3-Kolshi generation filter has a 100% Fe ° layer surmounted by a layer of sand. However, although presented as being very effective for the decontamination of arsenic, it has been shown to be limited in terms of the loss of porosity and rapid clogging. The Sono filter, made of a layer of porous materials, has a long lifespan, but is not very effective in decontaminating micropollutants, microorganisms, and viruses, and cannot reach the expected distribution; it will therefore be replaced by the KAF filter developed and distributed in Nepal. The latter, effective for arsenic and pathogens, has also been found to have limitations for certain classes of contaminants. Some systems have even been abandoned [22, 23].

To overcome rapid clogging and the short lifespan, sand (S), a material composed mainly of SiO_2, was combined with iron (Fe °) in a binary Fe °/S configuration, to aerate the reactive surface, but for partial remediation [24-27]. Non-expansive porous materials such as pozzolan (Pz) and natural charcoal (NC) help to unclog the reactive surface due to their absorption and adsorption ability. Indeed, Besides Fe °, the Fe °/S/Pz contains sand (S) and pozzolan (Pz). S is made up of 85% to 95% silica, an inorganic polymer SiO_2 or SiO_2, xH_2O, consisting of an assembly of silicic acid $Si(OH)_4$ molecules condensed in tetrahedral geometry. At pH > 2, silica has a negative charge on the surface, favoring the fixation of positively charged species. Silica is very often added to Fe ° to remedy the problem of chemical compaction of the Fe °-bed which causes the clogging of the pores [8, 28-32], generally caused by the CPs of Fe ° which are responsible for decontamination, among other things.

Pz is a material with various physicochemical characteristics. With a neutral pH, its average chemical composition is 45% SiO_2, 15% Al_2O_3, 15% Fe_2O_3, and other minor oxides [33]. It also contains lime, sodium, potassium, and many trace elements. The study of its physical characteristics reveals a high porosity, a low density, a capacity for absorbing water and odors, an aptitude for water retention, a large specific surface area, and a filtering and draining action, thus it has wide applications in the filtration and purification of water [34-36]. Its honeycomb structure and porosity give it a water absorption capacity of 20% to 30% of its dry weight [37]. Because of its

SiO_2 content, in addition to its high porosity, Pz has surface phenomena similar to those of S due to the silanol groups [29].

Fe °/S/Pz metal bed devices in a 25% Fe °/50%S/25%Pz configuration are partial decontaminants [24, 25]. The RZ with the proportions of 25%/50%/25% requires 40 g of material, which is not trivial, thus making its thickness dependent on the proportions of the materials [24]. Thus, nanoparticles (Np) with mirific adsorption and adsorption properties have been used for many techniques for the drinking and natural waters sanitation. Indeed, nanomaterials are nanometric particles whose size varies between 1 and 100 nm, with catalytic reactivity, thermal conductivity, optical performance, and even better chemical stability due to the volume-to-surface ratio [38]. They have properties related to their nanometric size, such as their specific surface area, surface reactivity and high oxidation-reduction activity [14, 39-41]. This is the case in this work of the silver nanoparticle based on *senna alata (SA)*, (AgNp), an herbaceous plant, an annual native to Mexico, but also found in Cameroon, Nigeria and Gabon. It has many properties such as antifungal, antibacterial, and corrosion inhibitory properties [15, 42-50].

This work consists of boosting a ternary Fe °/S/Pz device for electrochemical remediation of phosphates in waters, for improving the decontamination rate, while keeping almost intact the thickness of the RZ. To do this, a biosynthesis of a nanometric-sized AgNp based on *SA* is done, and only 0.5 g introduced into the RZ. Eighteen (18) filtering devices were tested for this, including six (6) 100% Fe °, (6) 25% Fe °/50% S/25% Pz, and (6) 25% Fe °/48.75% S/25% Pz/1.25% Np. A pollution indicator, phosphates, 0.2 g/L of K_2HPO4, at pH=5 close to the optimal pH of agricultural operations, was studied. Pollution parameters such as pH, decontamination rate, residual iron rate, flow rate; Conductivity and redox potential were measured.

2. Materials and Methods

2.1. Solutions

A solution of KH_2PO_4, 0.2 g/L, from ANALAR, is used in order to reconstitute a fraction of the N-P-K (Nitrogen-Phosphorus-Potassium) fertilizer. For the determination of phosphorus, a 50 mL / 200 mL H_2SO_4 solution from NORMAPUR is used to acidify the medium. The resulting H_3PO_4 reacts with a solution of ammonium molybdate $12(NH4)_2MoO_4$ from KERMEL, 2.5 g in 60 mL and allows the formation of the phosphomolybdic complex $(NH4)_3PO_4.12MoO_3$ catalyzed by potassium sodium tartrate, 0.137 g in 50 mL Ascorbic acid $C_6H_8O_6$ from E. MERCK, Darmstadt allows the reduction of the complex into a blue compound whose intensity and color are proportional to the concentration of phosphates. So the molybdic reagent consists of taking 200 mL H_2SO_4, 20 mL of potassium tartrate, 60 mL of ammonium molybdate, supplemented with 400 mL of distilled water. 2 mL of the yellow solution thus obtained, 10 mL of solution to be analyzed, 0.5 mL of $C_6H_8O_6$ gives a blue color. The reading is carried out after fifteen (15) minutes at 720 nm [58].

A standard iron solution, 990 µg/mL from Aldrich Chemical Company, Inc. (Milwaukee, WI, USA) was used to calibrate the spectrophotometer. The L (+) -ascorbic acid from E. MERCK, Darmstadt. 90% ethanol; sodium acetate from ANALAR; 1.10 o-phenanthroline from NORMAPUR used as a reagent for Fe^{2+} complexation require for spectrophotometric reading, 0.2 g/L concentration [51-53].

Four (4) materials were used to carry out our work, Table 1.

Table 1. *Granulometry, source, Symbol and nature of the materials used, [1]North Region, [2] South West Region, [3]Coastline Region, [4]Communal Market in Cameroon.*

N °	Materials	Symbol	Granulometry	Source	Nature
1	Sand	S	1 mm	Collected (NR^1)	Adsorbent
2	Pozzolan	Pz	2 mm	Collected (SWR^2)	Porous Absorbent/Adsorbent
3	AgNp *SA*	Np	1 nm	Collected (LR^3)	Porous Absorbent/Adsorbent
4	Fe^0	Fe °	≤ 1 mm	Collected (CM^4)	Adsorbent Generator

2.2. Solid Materials

2.2.1. Metal Iron

The iron used in this work is iron wool made by the steel mills of Cameroon (Douala, Cameroon) and marketed in the various local markets; its granulometry is less than 1 mm. This material has shown its effectiveness in discoloring methylene blue [6, 54]. It is used without treatment. The X-ray fluorescence analysis reveals: 0.62% Mn, 0.52% Si, 0.23% Cu, 0.2% Cr, and 0.09% Ni.

2.2.2. Sand and Pozzolan

The sand (S) used is a natural material taken in the Vina River (Cameroon), washed and rinsed with water boiled at 100 ℃ for 3 hours and then dried at 110 ℃ for 4 hours, it constitutes the different layers L_1 (upper), L_2 (intermediate or RZ) and finally L_3 (lower). For its availability and mixing agent, sand was used in Fe °/H_2O systems [7, 55]**.** The average chemical composition per X-ray diffraction reveals: 81.5% SiO_2, 5.60% Al_2O_3, 4.71% Fe_2O_3, 3.86% CaO, 1.75% TiO_2, 0.91% K_2O, 0.48% P_2O_5, 0.26% SO_3, 0.32% MnO, 0.08% SrO, 0.03% V_2O_5.

The pozzolan (Pz) used comes from Idenau (Southwest,

Cameroon) and has undergone the same pre-treatment as sand. It is L_2 layer (RZ). Pozzolan has a porosity of 60% which serves as a reservoir for Fe °CPs and has adsorption and absorption properties. The average chemical composition per X-ray diffraction is [33, 34]: 81.18% SiO_2, 10.00% Al_2O_3, 2.19% Fe_2O_3, 0.59% CaO, 0.46% TiO_2, 3.60% K_2O, 0.05% MnO, 0.02% SrO, 0.02% ZrO_2.

2.2.3. Silver Nanoparticle Based on Senna Alata (AgNp SA)

The leaves of *Senna alata* were harvested at the garden of the faculty of medicine and pharmaceutical sciences, coastline region in Cameroon, and authenticated at the National Herbarium of Cameroon by comparison with a specimen previously deposited under number 45, 146 / NHC (National Herbarium of Cameroon); then we proceeded as follows:

- Weigh 25 g of leaves previously washed and rinsed with distilled water.
- Introduce them into 250 mL of distilled water previously heated to 80 ℃.
- Keep the temperature of the mixture constant for five (5) minutes, then let the mixture rest for about four (4) minutes at room temperature.
- Filter and draw the absorbance curve A = f(λ).
- Prepare an $AgNO_3$ silver nitrate salt, adjust the pH to 8, then record the absorbance curve of the mixture, and compare it to the filtrate. Repeat this process until the ideal curve of the nanoparticle is obtained.
- Centrifuge to recover the crystals from the nanoparticle, then proceed with IR, UV, SEM, and XRD characterization as shown below [59, 60].
- Weigh 0.5 g of the silver nanoparticle thus synthesized and introduce it into the RZ of Fe °/S/Pz, in order to configure the Fe °/S/Pz/Np, a quaternary device, whose performance parameters we have evaluated through the elimination of phosphates.

Figure 1. *Senna Alata, N °45, 146/ NHC.*

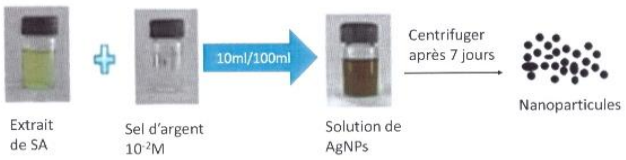

Figure 2. *Senna Alata synthesis.*

The chemical composition is determined by the contribution of MIPROMALO (Mission for the Promotion of Local Materials) in Yaounde- Cameroon. All the experiments concerning the synthesis of AgNp *SA* were carried out with the collaboration of the faculty of medicine of the University of Douala.

2.3. Procedure, Analytical Methods and Introducing Experimental Results

2.3.1. Procedure

We experimented with eighteen (18) filter devices including six (6) 100% Fe ° material devices, six (6) 25% Fe °/50% S/25% Pz devices, and six (6) 25% Fe °/48.75% S/25% Pz/1.25% Np quaternary devices. The column is made of polyethylene, and each filter has a total material mass of 220 g, including the top layer L_1 (m = 60 g of sand), intermediate layer L_2 (m = 40 g RZ) and lower layer L_3 (m = 120 g of sand). All devices are equal in total mass of materials.

Table 2. *Composition of the reactive zone (RZ) of each filtering device. The masses of materials are expressed in gram (g) and percentage (%).*

N °	Devices	Fe °(g)	Fe °(%)	S (g)	S (%)	Pz (g)	Pz (%)	Np (g)	Np (%)
1	Fe °	40	100	00	00	00	00	00	00
2	Fe °/S/Pz	10	25	20	50	10	25	00	00

N °	Devices	Fe °(g)	Fe °(%)	S (g)	S (%)	Pz (g)	Pz (%)	Np (g)	Np (%)
3	Fe °S/Pz/Np	10	25	19,5	48,75	10	25	0,50	1,25

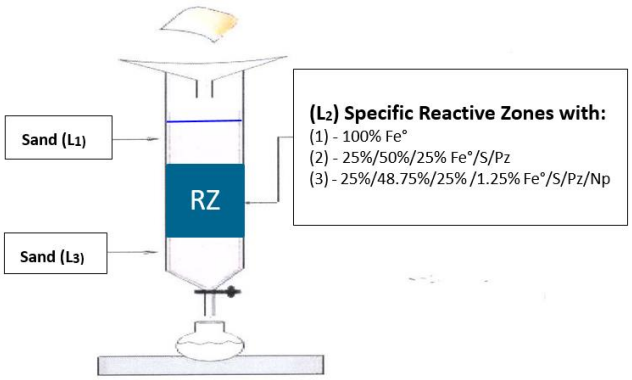

Figure 3. *Eighteen (18) experimental filtering devices, with specific Reactive Zones.*

L_1 ensures a distribution of raw water over the entire filtering device, decreases the energy or strength of the incoming contaminated water that can disturb the reactive layer, ensures the constant height of the polluted water; L_3, however avoids the phenomenon of air bubbles under the RZ, regularize or improve the flow [56].

2.3.2. Analytical Methods

The [Fe] wavelength of phosphates is 720 nm, and for the iron solution is 510 nm. The reading was done by a JENWAY brand UV-Vis spectrophotometer of model 6715. METTER TOLEDO S 470 allows the measurement of pH, conductivity, and redox potential. FTIR (Fourier Transform Infrared) spectroscopy was conducted using a Bruker Tensor 37. XRD (X-ray Diffraction) was performed using a Bruker D2 phaser powder diffractometer (Cuk- [Å] 1.54060, K-Alpha2 [Å] 1.54443, K- Beta [Å] 1.39225) by preparing a thin film on a low background silicon sample holder.

2.3.3. Introducing Experimental Results

The effectiveness in discoloring the initial phosphates filter (c_o) depending on the residual phosphate ions content, the effectiveness (E) to discoloration is given by the relationship:

$$E(\%) = \left(1 - \frac{Ce}{Co}\right) \times 100.$$

Residual iron is determined according to the 1.10 Orthophenanthroline protocol [57]. The UV-Vis spectrophotometer is read at λ = 510 nm and λ = 720 nm for phosphates.

3. Results

100% Fe °-Bed Filtering Power and the Removal Rate of Phosphate Ions in Collected Waters

Figures 4, 5, 6, 7, 8 and 9 depict the results obtained for a 100% Fe °RZ, in the presence of a pollution indicator, phosphate ions, at pH = 5. Indeed, the RZ is sandwiched between the L_1 and L_3 layers, as shown in Figure 3.

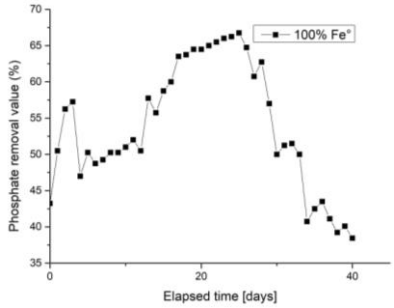

Figure 4. *Phosphates removal values, one-material RZ with pure Fe °, 100% Fe °.*

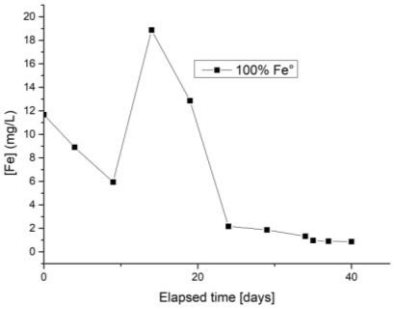

Figure 5. *[Fe] released iron, one-material RZ with pure Fe °, 100% Fe °.*

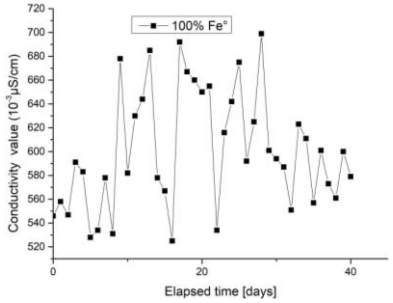

Figure 6. *Conductivity study, one-material RZ with pure Fe °, 100% Fe °.*

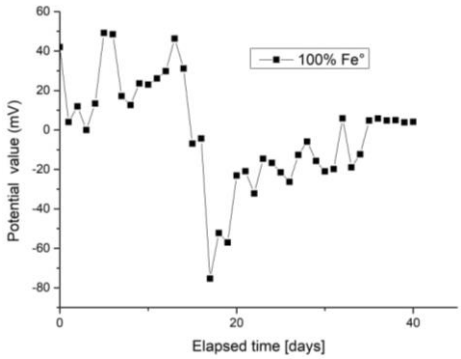

Figure 7. *Potential redox study, one-material RZ with pure Fe °, 100% Fe °.*

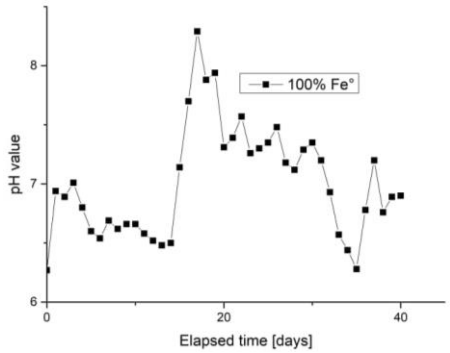

Figure 8. *Ph study, one-material RZ with pure Fe °, 100% Fe °.*

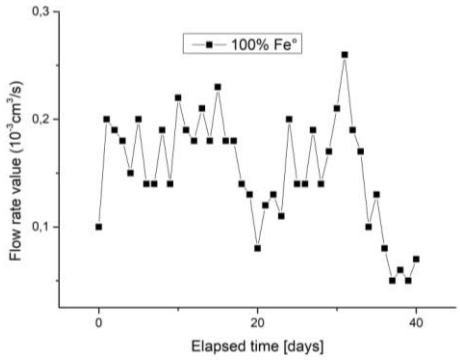

Figure 9. *The flow rate, one-material RZ with pure Fe °, 100% Fe °.*

Biosynthesis of AgNps SA and Enhancement of 25% Fe ℅ 50% S/25% Pz for 25% Fe ℅48.75% S/25% Pz/1.25% Np

The leaves of *Senna alata (SA)* Figure 1, were harvested at the garden of the faculty of medicine and pharmaceutical sciences, coastline region in Cameroon, and authenticated at the National Herbarium of Cameroon (NHC) by comparison first with a specimen previously deposited under number 45, 146 / NHC, then by physico-chemical characterization using XRD (X-ray Diffraction) and FTIR (Fourier Transform Infrared) spectroscopy, withing the laboratory of the faculty of pharmacy. The following devices were respectively used for this purpose. FTIR (Fourier Transform Infrared) spectroscopy was conducted using a Bruker Tensor 37. XRD (X-ray Diffraction) was performed using a Bruker D2 phaser powder diffractometer (Cuk-[Å] 1.54060, K-Alpha2 [Å] 1.54443, K-Beta [Å] 1.39225) by preparing a thin film on a low background silicon sample holder, as already mentioned in paragraph 2.4 above. The synthesis was done according to the protocol described in paragraph 2.2.4, as shown in Figure 2.

Nanoparticles thus synthesized and characterized, are introduced into the RZ of 25% Fe ℅50% S/25% Pz, in order to set up a quaternary device 25% Fe ℅48.75% S/25% Pz/1.25% Np. The modus operandi has been detailed above as shown in Figure 3. Figures 10, 11, and 12 are the results obtained from the synthesis of AgNps *SA*. Figure 10 is the UV spectrum of the silver nanoparticle. A stable characteristic peak of spherical nanoparticles is observed at 420 nm.

Figures 13, 14, 15, 16, 20, and 21 depict the performance of the ternary filtering system modified by AgNps 25% Fe ℅ 48.75% S/25% Pz/1.25% Np.

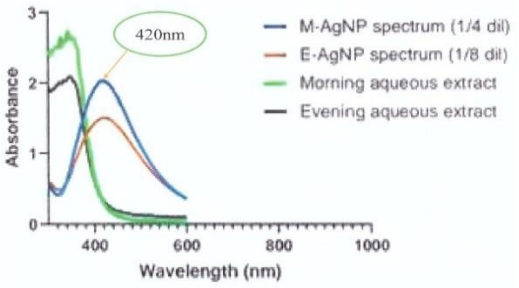

Figure 10. *UV Spectroscopy of AgNp SA.*

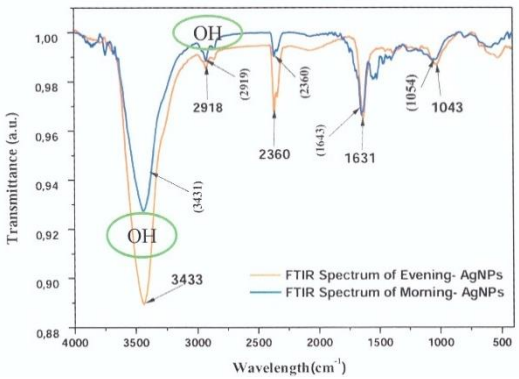

Figure 11. *FTIR Spectroscopy of AgNp SA.*

Table 3. FTIR Spectroscopy of AgNp SA, following figure 11.

M-AgNPs Frequencies (cm^{-1})	E-AgNPs Frequencies (cm^{-1})	Functional group	Type of vibrations
3431	3433	O-H	Stretching vibrations (Alcohols and phenols)
2919	2918	C-H	Stretching vibrations (Aromatic compounds (Coumarins, Flavonoids, alkaloids, salicylic acid, ….)
2360	2360	O=C=O	Stretching vibrations (Carbonyl bond group)
1643	1631	C-N C-C	Stretching vibrations (Proteins, Primary amines)
1537	/	N-H	Bending vibrations(Secondary amines)
1054	1043	C-H	Bending vibrations (Aromatic alkanes, alkenes and Alkynes and aromatic hydrocarbons)

Table 4. XRD of AgNp SA following figure 12.

Important Peaks	Miller Indices (hkl)	Position (2 θ) AgNPs	Angle θ (radian)	FWHM (Radian)	Diameter (nm)
1	111	38.07	0.3316	0.6571	13.36
2	200	44.15	0.384	0.6571	13.32
3	220	64.42	0.5585	0.6671	14.58
4	311	77.31	0.6632	0.6671	15.80

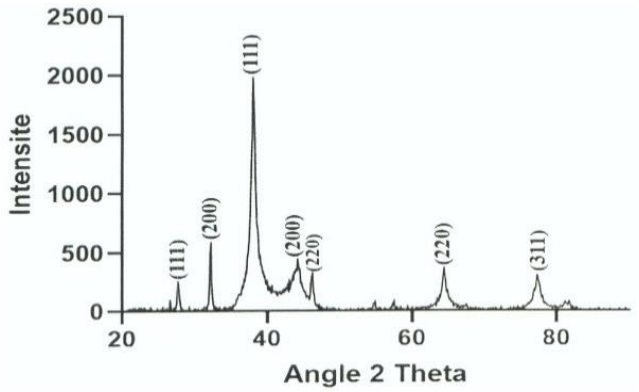

Figure 12. XRD of AgNp SA.

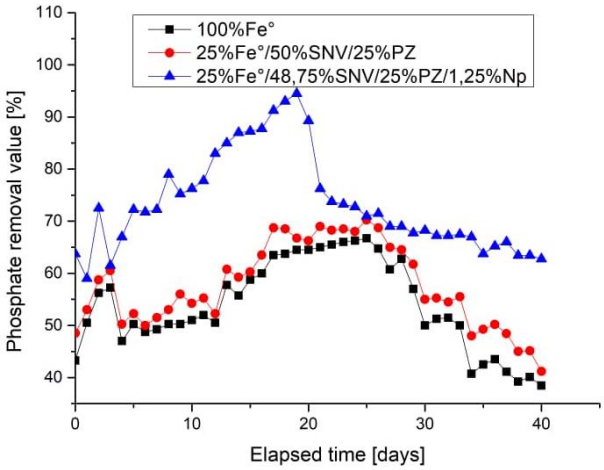

Figure 13. Performance of quaternary device 25%/48.75/25%/1.25% Fe ?S/Pz/Np for phosphate ions removal.

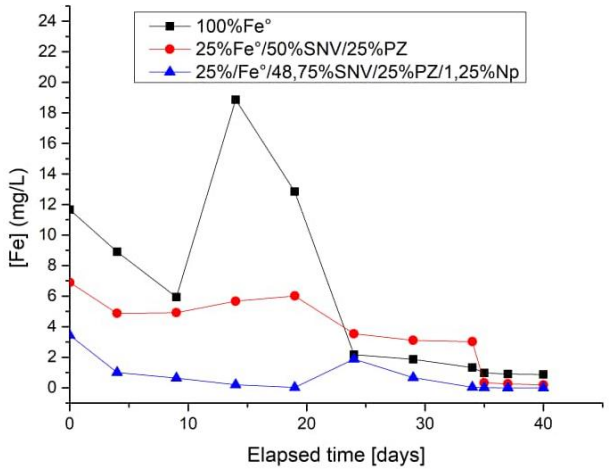

Figure 14. *Performance of quaternary device 25%/48.75/25%/1.25% Fe °S/Pz/Np for removal of dissolved iron.*

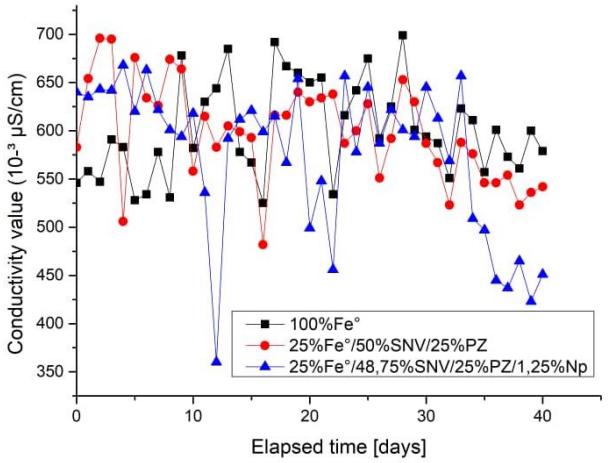

Figure 15. *Conductivity studies, with Fe °, Fe °S/Pz and 25%/48.75/25%/1.25% Fe °S/Pz/Np RZs.*

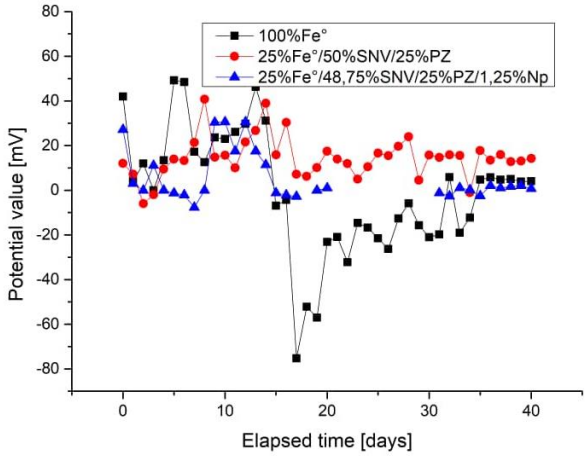

Figure 16. *Redox potential studies, with Fe °, Fe °S/Pz and 25%/48.75/25%/1.25% Fe °S/Pz/Np RZs.*

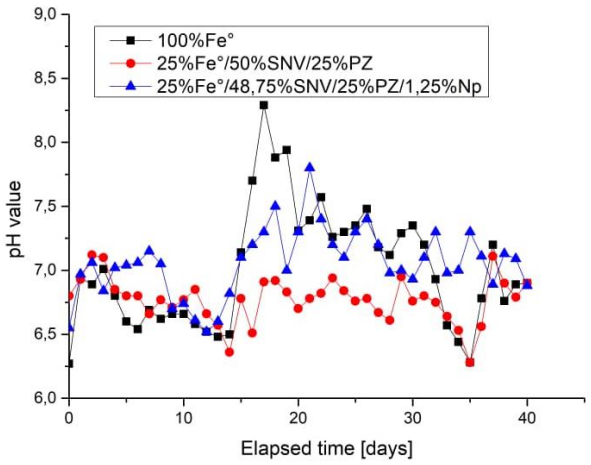

Figure 17. *Performance of quaternary device 25%/48.75/25%/1.25% Fe °S/Pz/Np for pH adjustment.*

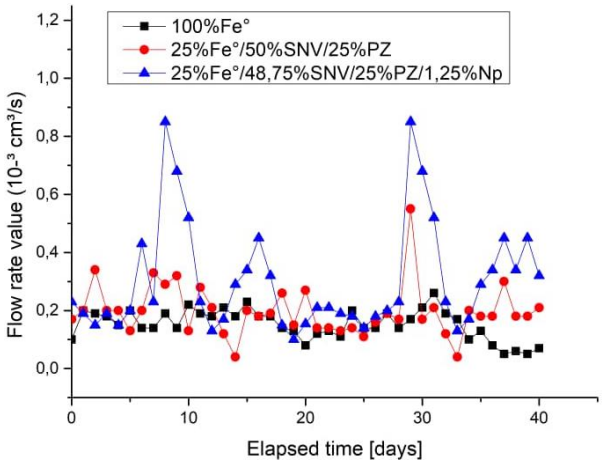

Figure 18. *Performance of quaternary device 25%/48.75/25%/1.25% Fe °S/Pz/Np on throughput improvement.*

4. Discussion

100% Fe °-Bed Filtering Power and the Removal Rate of Phosphate Ions in Collected Waters

Figure 4 shows a removal rate of up to 65%. There would therefore be a real affinity between the phosphate ions and the filter column, despite the surface reactivity of the S, due to the presence of the silanol groups of the L_1 and L_3 layers. However, a loss of responsiveness occurs beyond twenty (20) days. This is on the one hand in agreement with the work of Harza [21], since 100% Fe ° is subject to rapid clogging, which impacts their lifetime, and on the other hand, validates our work on the imperative need to support Fe °by the association of non-expansive porous materials such as Pz and NC [24-27]. The presence of Fe^{2+} ions in the harvested water, Figure 5, is evidence of Fe °oxidation. However, the [Fe] remains low and corroborates those of the conductivity, Figure 6, and the very low values close to zero of the redox potential, [0.04V;

-0.08V], Figure 7, due to the pH of the collected water, Figure 8, whose values vary from 5 to 7.5 on average, which is proof of the elimination of phosphates. The Cps of Fe ° therefore ensure a decontamination process, and the flow rates measured in Figure 9 allow for good recovery.

However, the low removal rate, loss of porosity and reactivity of 100% Fe ° led to the introduction of other materials into the RZ, namely the ternary 25% Fe °/50% S/25% Pz. Although there is an improvement compared to 100% Fe °, the loss of reactivity still occurs beyond twenty (20) days, and decontamination is partial. Hence the need to introduce a material that can increase the reactive surface and inhibit corrosion.

Biosynthesis of AgNps SA and Enhancement of 25% Fe °/ 50% S /25% Pz for 25% Fe °/48.75% /25% Pz /1.25% Np

Figure 10 is the UV spectrum of the silver nanoparticle. A stable characteristic peak of spherical nanoparticles is observed at 420 nm. Thus, the green synthesis of AgNp from aqueous extracts of *SA* was confirmed as described by Song & al. [67], and Iravani [68].

Figure 11 is the FTIR spectrum of AgNps SA and reveals a number of bands in the same range as AgNps. FTIR Spectroscopy is based on the absorption of Infrared radiation by material being analyzed. The different vibrations observed are characteristic of the biomolecules present as shown in Table 3. The stretches observed around 3431 cm^{-1} correspond to the presence of O-H vibrations of phenols and alcohols. Those around 2919 cm^{-1} can be attributed to C-H vibration stretches of the aromatic compounds as shown in Table 3; The peak at 2360 cm^{-1} corresponds to carbonyl vibrations, while the peak at 1643 cm^{-1} corresponds to primary amines, and 1537 cm^{-1} to secondary amines. 1054 cm^{-1} can also be attributed to bending vibrations of aromatic alkanes, alkenes, alkynes and aromatic hydrocarbons. This characterization shows the metabolites of the nanoparticle, and the vibrations observed are in line with the literature [69].

Figure 12 shows X-ray diffraction, an analytical technic that provides information on the structure and phase identification of crystalline materials, by comparison with spectra of reference compounds. Indeed, many studies have shown that AgNps have a cubic structure with peaks at 38.06 °, 44.22 °, 64.48 ° and 77.32 ° corresponding to the 2ɵ angle of planes (111), (200), (220) and (311) respectively. Figure 12 of the AgNps XRD shows that the diffraction pattern occurs at 38.07 °, 44.15 °, 64.42 ° and 77.31 ° (2ɵ); These models can be indexed to the (111), (200), (220), and (311) face-centered cubic silver plans as shown in Table 4, [61, 62, 70].

Figures 13, 14, 15, 16, 17, and 18 depict the performance of the ternary filtering system modified by AgNps 25% Fe ° / 48.75% S / 25% Pz / 1.25% Np. It appears that the decontamination rate of 100% Fe °device is very close to that of the ternary 25% Fe ° / 50% S / 25% Pz in the absence of AgNp. This is due to the reduction in the proportion of Fe ° from 100% to 25% on the one hand, and then to the low affinity of anions with regard to sand and pozzolan composed mainly of silica SiO_2 on the other hand, and whose surface reactivity would repel phosphate ions, which are anionic pollutants [21, 24-27, 63-66]. S is made up of 85% to 95% silica, an inorganic polymer SiO_2 or SiO_2, xH_2O, consisting of an assembly of silicic acid $Si(OH)_4$ molecules condensed in tetrahedral geometry. At pH > 2, silica has a negative charge on the surface, favoring the fixation of positively charged species [8, 28-32].

Thus, Figure 13 shows that the introduction of 1.25% of AgNps in the RZ has led to an extraordinary increase in reactivity, due to the small quantity tested. Indeed, with 1.25% of AgNps SA, and 20 times more Fe °, 39 times more S, and 20 times more Pz, the phosphate removal rate increases, and the lifetime of Fe/S/Pz is extended.

This is due to the nanometric size of AgNps, their large specific surface area, and their adsorption properties which, combined with Fe °, allow an improvement in Fe °/S/Pz such as Fe ° < 25% Fe °/50% S/25% Pz < 25% Fe °/48.75% S/25% Pz/1.25% Np. They also promote better interaction with phosphate ions in accordance with research work of Zhang & al. [71]. The performances of 25% Fe °/48.75% S/25% Pz/1.25% Np are agreement with the work of Liu & al. who showed that Ag-Fe (nanocomposite) association is efficient for oxygenated anions [77].

Figure 14 confirms the adsorption properties of AgNps, since the concentration of [Fe] in the harvested water is almost zero, 25% Fe °/48.75% S/25% Pz/1.25% Np < 25% Fe °/50% S/25% Pz < Fe °. Compared to 100% Fe °, this reflects an improved control of iron oxidation products release, as also highlighted by Liu & al. [72].

The measured conductivity values remain low, Figure 15, this shows adequate electrolytic stability and limited release of undesirable ionic compounds. This behavior is consistent with a mechanism of selective adsorption and enhanced precipitation. The values of the redox potentials measured in Figure 16, which are almost zero, corroborate those of Figure 14, the elimination of residual Fe °, and those of Figure 17, since the 6.8≤ pH ≤8.3 with the 25% Fe °/48.75% S/25% Pz /1.25% Np. According to Zhang & al. [75], AgNps promote electron exchange because can serve as an electron bridge, facilitating the controlled corrosion of Fe °, and the generation of reactive species like Fe^{2+}, Fe^{3+}.

The pH is different from the initial pH of the solution, and reflects the removal of phosphate ions, either by affinity with the Cps [24-32], or by adsorption [73].

Thus, Figures 19 and 20 depict the Pourbaix diagrams of the Fe ° and Ag °. They show that Fe ° is oxidizable in contact with water, which generates Cps. Indeed, the immunity domain of Fe ° is below the stability domain of water, which means that Fe °can be oxidized by O_2, but especially by water, since we work in an anoxic environment, the RZ being sandwiched between the L_1 and L_3 layers.

Figure 20 shows that the immunity domain of Ag partially covers the stability domain of water [19, 20], and cannot be oxidized by water, but can be oxidized by O_2, which is not the case for 25% Fe °/48.75% S/25% Pz/1.25% Np. Fe ° and AgNps coexist perfectly in the RZ, and the Cps of Fe ° contribute to the

decontamination process. Moreover, the presence of polyphenols in the extract also acts in the stabilization of Ag°. Indeed, the synthesis of AgNps by biological entities is due to a large number of organic molecules, in particular polyphenols, Figure 21. Polyphenols are adsorbed to the surface of AgNps to stabilize them; they play a dual role of reductive and stabilizer [78].

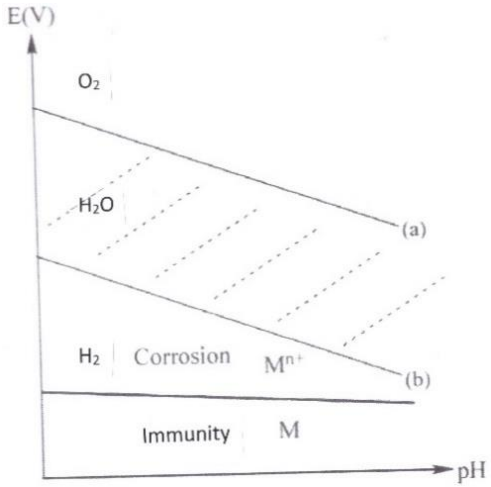

Figure 19. *Pourbaix Diagram of Fe°.*

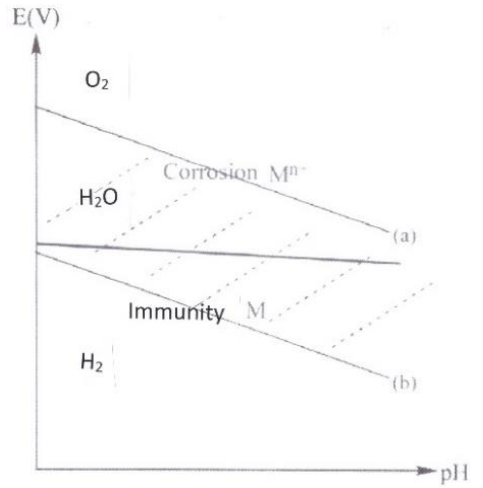

Figure 20. *Pourbaix Diagram of Ag.*

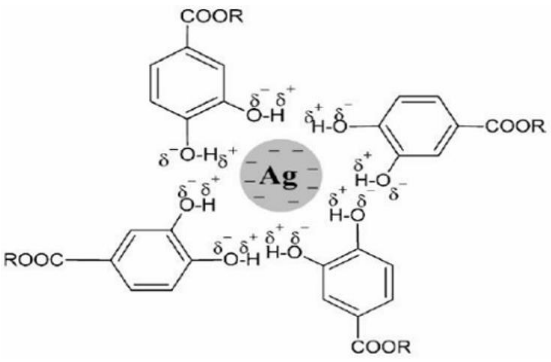

Figure 21. *Ag stabilization mechanism.*

Figure 18 shows that the introduction of AgNps into the RZ does not deteriorate the flow, which is rather constant and acceptable. No hydraulic resistance is observed due to the presence of AgNps [74]. In addition, the ant-microbial effects of AgNps is proven. What inhibits bacterial growth, reduces bio clogging and loss of hydraulic conductivity. Rai & al. have shown the effective inhibition of AgNps on a broad microbial spectrum via enzymatic denaturation and membrane peroxidation [76].

One of the major advantages of the configuration of 25% Fe°/48.75% S/25% Pz/1.25% Np, in addition to the reactivity, the extension of the lifespan, the removal of released iron, the fit of the pH according to the recommendations of the WHO, is that the thickness of the RZ is not modified, which requires very little product unlike other non-expansive porous materials such as Pz, or the NC [24-27]. The decontamination process of Fe°-based filters/NPS is therefore based on the oxidation of Fe° and its Cps. AgNps and Pz are adsorbent materials that can support the reactivity of Fe° in the RZ.

5. Conclusion

This work consisted of the biosynthesis of AgNp SA to overcome the limits of a Fe°/S/Pz, and the removal of phosphates, anionic pollutants. To do this, we introduced 1.25% AgNp SA in the RZ for a 25% Fe°/48.75% S/25% Pz/1.25% Np. Eighteen (18) devices were tested, (6) 100% Fe°, (6) 25% Fe°/50% S/25% Pz and (6) 25% Fe°/48.75% S/25% Pz /1.25% Np, on water polluted with phosphate ions. The results obtained show that Fe° alone is subject to rapid clogging. The modification of the RZ of a 25% Fe°/50% S/25% Pz device by the introduction of 1.25% of AgNp SA, allows to boost the Fe°/S/Pz. There is a revival of reactivity, the rate of pollutant removal is increased, clogging is delayed, the residual ferrous ions level is almost zero, the thickness of the RZ is not modified. Thus, Fe° < 25% Fe°/50% S/25% Pz < 25% Fe°/48.75% S/25% Pz/1.25% Np. These results are consistent with our previous work. Indeed, 25% Fe°/50% S/25% Pz devices allow to reduce greatly the proportion of iron in the RZ since 100% Fe°-bed filters are not recommended due to clogging, and 25% ≤%Fe°≤ 60% could provide a necessary framework for all Fe°-bed filters. Since it is necessary to avoid 100% Fe° in the RZ, the most durable filters contain no more than 25% Fe°. Moreover, Ag° is stable due to immunity domain towards water according to the Pourbaix diagram, but also due to its stabilization by polyphenols. Only Fe° is corroded, so that Pz and AgNp act as adsorbent materials and support the reactivity of Fe°-bed filters. So, the association of AgNp for a Fe°/S/Pz/Np quaternary device allows us to achieve our objectives in terms of agricultural products sanitation.

6. Recommendations

Nanoparticles have multiple benefits listed in this manuscript, including their antibacterial properties. A complete filtering system must ensure both a physicochemical and bacteriological decontamination process. It therefore recommends that research work be continued in this direction.

Abbreviations

Ag °	Ag, Ag (0), Silver (0)
Cps	Corrosion products
Fe °	Fe, Fe (0), Iron (0)
Np	Nanoparticle
AgNp	Silver Nanoparticles
Pz	Pozzolan
S	Sand
SA	*Senna Alata*
RZ	Reactive Zone
Fe °/S/Pz	Iron/Sand/Pozzolan
Fe °/S/Pz/Np	Iron/Sand/Pozzolan/Nanoparticle
WHO	World Health Organization
NC	Natura Coal

Acknowledgments

Our thanks to the Department of Chemistry of the Faculty of Science, University of Douala, to the Department of Chemistry of the Faculty of Medicine, University of Douala, and finally to the Department of Applied Geology, University of Göttingen for their unwavering support at all times. Thanks to MIPROMALO-Cameroon for the characterization of materials.

Conflicts of Interest

The authors declare no conflicts of interest.

References

[1] Ebelle, T. C., Makota, S., Tepong-Tsindé, R., Nassi, A., & Noubactep, C. August (2016). Metallic iron and the dialogue of the deaf. Fres. Environ. Bull. 28 (11A): 8331-8340.

[2] Makota, S., Ndé-Tchoupé, A. I., Mwakabona, H. T., Tepong-Tsindé, R., Noubactep, C., Nassi, A., & Njau, K. N. (2017). Metallic iron for water treatment: leaving valley of confusion. Appl. Water Sci. 7: 4177-4196.

[3] Noubactep, C., Makota, S., & Randyopadhyay, A. (2017). Rescuing Fe ° remediation research from its systemic flaws. Res. Rev. Insights 1 (4): 1-8.

[4] Ndé-Tchoupé, A. I. Crane, R. A., Mwakabona, H. T., Noubactep, C., & Njau, K. (2015). Technologies for decentralized fluoride removal: Testing metallic iron -based filters. Walter 7: 6750-6774.

[5] Nasseri, E., Ndé-Tchoupé, A. I., Mwakabona, H. T., Nanseu-Njiki, C. P., Noubactep, C., Njau, K. N., & Wydra, K. D. (2017). Making Fe °-based filters a universal solution for safe drinking water provision. Sustainability 9: 1224.

[6] Noubactep, C. (2009). An analysis of the evolution of reactive species in Fe °/H_2O systems. J. Hazard Mater 168: 1626- 1631.

[7] Anderson, W. (1885). The purification of water by means of iron on the large scale. Minutes of the Proceedings of the Institution of Civil Engineers 81: 279-284.

[8] Henderson, A. D., & Demond, A. H. (2007). Long-term performance of zero-valent iron permeable reactive barriers: a critical review. Environ. Eng. Sci. 24: 401-423.

[9] Gheju M. (2011). Hexavalent chromium reduction with zero-valent iron (ZVI) in aquatic systems Water Air Soil Pollut. 222: 103-148.

[10] Noubactep, C. (2010a). The fundamental mechanism of aqueous contaminant removal by metallic iron. Water SA 36, 663-670.

[11] Noubactep, C. (2006). Contaminant reduction at the surface of elemental iron: The end of a myth. Wissenschaftliche Mitteilungen Freiberg 31: 173-179.

[12] Noubactep, C. (2008). Processes of contaminant removal in 'Fe°-H_2O' systems revisited: The importance of co-precipitation. Open Environ. Sci. 1: 9-13.

[13] Noubactep, C. (2013a). Relevant reducing agents in remediation Fe °/H_2O systems Clean-Soil Air Water 41: 493-502.

[14] Miyajima, K. (2012). Optimizing the design of metallic iron filters for water treatment. Freiberg Online Geosci. 32: 107.

[15] Noubactep, C. (2010b). Metallic iron for safe drinking water worldwide. Chem. Eng. J. 165: 740-749.

[16] Pilling, N. B., &Bedworth, R. E. The oxidation of metals at high temperatures. J. Inst. Metals (1923). 29: 529, 591.

[17] Crawford, R. J., Harding, I. H., & Mainwaring, D. E. (1993a). Adsorption and coprecipitation of single heavy metal ions onto the hydrated oxides of iron and chromium. Langmuir 9: 3050-3056.

[18] Schwertmann, U. (1991). Solubility and dissolution of iron oxides. Plants and Soil 130: 1-25.

[19] Lamoureux, J-J. (2000). Précis de corrosion. Sciences des matériaux p. 1-78, (2e Eds) Masson.

[20] Detay, M. (1993). Le forage de l'eau. Ingénierie de l'environnement p. 231-242, (Eds) Masson (In French).

[21] Harza Engineering Co. (1986). Selenium removal study, Report to Panoche Drainage District. Harza Engineering Co., Firebaugh, California, USA.

[22] Ngai, T. K. K., Shrestha, R. R., Dangol, B., Maharjan, M., & Murcott, S. E. (2007). Design for sustainable development - Household drinking water filter for Arsenic and pathogen treatment in Nepal. J. Environ. Sci. Health 42: 1879-1888.

[23] Munir, A. K. M., Rasul, S. B., Habibuddowla, M, Hussam, A., & Khan, A. H. (2001). Evaluation of performance of filter for arsenic removal from groundwater using zero-valent iron through laboratory and field studies. Technologies for arsenic removal from drinking water. 171 - 189.

[24] Suzanne Makota, S. N., Nguemo Wekam, E. A., Dipita Kolye, E. Y. H. & Nassi, A. (2022). Ranges and Fitting Ratios of Natural Aggregates for a Sustainable and Effective Fe°/Sand/Pozzolan ternary Device Using Oranges Methyl. American Journal of Applied Chemistry. Vol. 10, No 1, pp. 15-27. https://doi.org/10.11648/J.ajac.20221001.13 ISSN: 2330-8753 (Print); ISSN: 2330-8745 (Online).

[25] Ndé-Tchoupé, A. I., Makota, S., Nassi, A., Rui, H., & Noubactep, C. (2018). The suitability of pozzolan as admixing aggregate for Fe°-Based Filters. Water 10: 417.

[26] Suzanne Makota S. N., & Dipita Kolye, E. Y. H. (2021). Natural Coal Aggregates to the Rescue of Fe°-Bed Filters in Quaternary Reactive Zones Fe°/S/Pz/C_X to Repel Clogging and Boost Reactivity. American Journal of Applied Chemistry. Vol. 9, No. 3, pp. 74-82. https://doi.org/10.11648/j.ajac.20210903.13 ISSN: 2330-8753 (Print); ISSN: 2330-8745 (Online).

[27] Dipita Kolye, E. Y. H., Suzanne Makota, S. N., Mbarga, L. V., Mintang Fongang, U. A., Dika Manga, J. M & Nassi, A. (2022). Natural Charcoal in Water Treatment Through Metal Bed Filters Fe°/S/Pz: The Concept of Wood-Energy-Sanitation. American Journal of Applied Chemistry. Vol. 10, No 1, pp. 28-37. https://doi.org/10.11648/J.ajac.20221001.14 ISSN: 2330-8753 (Print); 2330-8745 (Online).

[28] Anderson, W. (1896). On the purification of water by agitation with iron and by sand filtration. Journal of the Society for Arts 35 (1775): 29-38.

[29] Iler, R. (1979). The Chemistry of Silica. Wiley Intersci. Public. 35 pp. New York, USA.

[30] Miyajima, K., & Noubactep, C. (2012). Effects of Mixing Granular Iron with Sand on the Efficiency of Methylene Blue Discoloration. Chem. Eng. J 433-438.

[31] Wilkin, R., Puls, R., & Sewell, G. (2003). Long-term performance of permeable reactive barriers using zero-valent iron: geochemical and microbiological effects, Ground Water 41: 493-503.

[32] Mitchell, G., Poole, P., Segrove, H. (1955). Adsorption of Methylene Blue by High-Silica Sands. Nature 176: 1025-1026.

[33] Dron, R. (1975). Les pouzzolanes et la pouzzolanicité. Revue des matériaux de construction (In French). N°692: 27-30.

[34] Kofa, G. P., NdiKoungou, S., Kayem, G. J., Kamga, R. (2015). Adsorption of arsenic by natural pozzolan in a fixed bed: determination of operating conditions and modeling. J. Water Process Eng. 6: 166-173.

[35] Billong, N., Chinje Melo U., Njopwouo, D., Louvet, F., & Bonnet, J. P. (2013). Physicochemical characteristics of some Cameroonian pozzolans for use in sustainable cement like materials. Materials Sci. Appl. 4: 14-21.

[36] Sieliechi, J. M., Lartiges, B. S., Ndi, S. K, Kamga, R., & Kayem, G. J. (2012). Mobilization of heavy metal from natural pozzolan by humic acid: implications for water and environment, Int. J Environ. 2: 11-15.

[37] Rocher, P. (1992). Mémento roches et minéraux industriels. Ponces et pouzzolanes. Rapport BRGM, R 36447: 21-22, 45.

[38] Phukan, M. (2015). Characterizing the Fe°/sand system by the extent of dye discoloration. Freiberg Online Geosci. 40: 70.

[39] Comba, S., Di Molfetta, A., Sethi, R. (2011). A Comparison between field applications of nano-, micro-, and millimetric zero-valent iron for the remediation of contaminated aquifers. Water Air Soil Pollut 215: 595-607.

[40] Yao, K. M., Habibian, M. T., & O'melia, C. R. (1971). Water and wastewater filtration: concepts and applications. Environ. Sci. Technol. 5: 1105-1112.

[41] Howe, K. J., Hand, D. W., Crittenden, J. C., Trussel, R. R., Tchobanoglous, G. (2012). Principles of water treatment. John & Wiley Sons, Inc., Hoboken, New Jersey, 674.

[42] Seng, C. L., Yang, M. H., &Lin, C. C. (1984). Rapid determination of cobalt-60 in sea water with steel wool adsorption. J. Radioanal. Nuclu. Chem. Lett. 85: 253-260.

[43] James, B. R., Rabenhorst, M. C., & Frigon, G. A. (1992). Phosphorus sorption by peat and sand amended with iron oxides or steel wool. Water Environ. Res 64, 699-705.

[44] Bischof, G. (1878). On putrescent organic matter in potable water. II. Proceedings of the Royal Society of London 27: 258-261.

[45] Lackovic, J. A., Nikolaidis, N. P., & Dobbs, G. M. (2000). Inorganic arsenic removal by zero-valent iron. Environ. Eng. Sci. 17: 29-39.

[46] Bigg, T., Judd, S. J. (2000). Zero-valent iron for water treatment. Environ Technol. 21: 661-670.

[47] Prosie, F. Lesage, F. X. & Deschamps F. (2008). La nanoparticule: structures, utilisations et effets sur la santé. La presse Médicale. 37: 1432 (In French).

[48] Khan, I., Saeed, K. & Idrees, K. (2019). Nanoparticles: Properties, Applications and toxicities. Arabian Journal Chemistry. 908-993.

[49] Borm, P. J., Robbins, D., Haubold, S., Kuhlbusch, T., Fissan, H., Donaldson, K., Schins, R., Stone, V., Kreyling, W. & Lademann J. (2006). Particle and fibre toxicology.

[50] Angelique, S. D., Audureau, E., Franco, M. et al. (2018). Substantial of the gene expression profile following exposure of macrophages to welding-related nanoparticles. J. Sci. Rep.; 4; 8(1): 8554. https://doi.org/10.1038/s41598-26988-z

[51] Norme NF T 90-017. (1982). Dosage du fer, Méthode spectrométrique à la phénanthroline-1, 10, AFNOR Paris (In French).

[52] Rejsek, F. (2002). Analyse des eaux - Aspects réglementaires et techniques p. 66 (In French).

[53] Standard Methods for the examination of water, 19th edition, sheet 3-68.

[54] Noubactep, C. (2016b). Designing metallic iron packed - beds for water treatment: Acritical review. CLEAN – Soil, Air, Water. 44: 411- 421.

[55] Devonshire, E. (1890). The purification of water by means of metallic iron. Journal of the Franklin Institute 129: 449-461.

[56] Centre International de l'eau et de l'assainissement IRC/ (1991). la filtration lente sur sable pour approvisionnement en eau potable (In French).

[57] Fortune, W. B., & Mellon, M. G. (Ed. 1938). Determination of iron with o-phenanthroline: A spectrophotometric study. Ind. Eng. Chem. Anal. 10: 60-64.

[58] Rodier, J., Legube, B., Merlet, N. et coll. (2009). 9ème édition, Dunod, Paris. Pp 388.

[59] Eya'ane, F., Ebongue, C. O., Fannang, S. V., Segnou, M. L., Ntoumba, A. A., & Belle P. (2017) « Natural Substances for the Synthesis of Silver Nanoparticles against Escherichia coli: The Case of Megaphrynium macrostachymum (Marantaceae), Corchorus olitorus (Tiliaceae), Ricinodendron heudelotii (Euphorbiaceae), Gnetum bucholzianum (Gnetaceae) & Ipomoea batatas (Convolvulaceae). Journal of Nanomaterials. 1: 1-6.

[60] Hassan, P. A. & Kulshreshtha, S. K. (2006). " Modification to the cumulant analysis of polydispersity in quasielastic light scattering data". Journal of colloid and interface Science. 300: 740-750.

[61] Syafiuddin, A., Salim, M. R., Beng Hong kueh, A., Hadibarata, T. & Nur, H. (2017). A review of silver nanoparticles: research trends, global consumption, synthesis, properties & future challenges. Journal of the Chinese Chemical Society. 64 (7); 732-756.

[62] Subapriyal, M. R. (2012). "Green Synthesis of silver nanoparticles". International Journal of Pharma medicine and biological sciences Vol. 1, n °1: 2278-5221.

[63] Rahman, M. A., Karmakar, S., Salama, H., Gactha-Bandjun, N., Btatkeu-K, B. D., & Noubactep, C. (2013). Optimising the design of Fe(0)-based filtration systems for water treatment: The suitability of porous iron composites. J. Appl. Solut. Chem. Model. 2: 165-177.

[64] Btatkeu-K, B. D., Olvera-Vargas, H., Tchatchueng, J. B., Noubactep, C., & Caré, S. (2014). Determining the optimum Fe °ratio for sustainable granular Fe %sand water filters. Chem. Eng. J. 247: 265-274.

[65] Bilardi, S., Calabrò, P. S., Caré, S., Moraci, N., & Noubactep, C. (2013a). Improving the sustainability of granular iron/pumice systems for water treatment. J. Environ. Manag. 121: 133-141.

[66] Bilardi, S., Calabrò, P. S., Caré, S., Moraci, N., & Noubactep, C. (2013b). Effect of pumice and sand on the sustainability of granular iron beds for the removal of Cu^{II}, Ni^{II}, and Zn^{II}. Clean-Soil Air Water 41: 835-843.

[67] Song, J. Y. & Kim, B. S. (2009). Rapid biological synthesis of silver nanoparticles using plant leaf extracts. Journal of Nanoparticle Research, 11(1), 1-8. https://doi.org/10.1007/s11051-008-9443-1

[68] Iravani, S. (2011). Green synthesis of metal nanoparticles using plants. Green Chemistry, 13(10), 2638-2650. https://doi.org/10.1039/C1GC15386B

[69] Mittal, A. K., Chisti, Y., & Banerjee, U. C. (2013). Synthesis of metallic nanoparticles using plant extracts. Biotechnology Advances, 31(2), 346-356. https://doi.org/10.1016/j.biotechadv.2013.01.003

[70] Narayanan, K. B. & Sakthivel, N. (2010). Biological synthesis of metal nanoparticles by microbes. Advances in Colloid and Interface Science, 156(1-2), 1-13. https://doi.org/10.1016/j.cis.2010.02.001

[71] Zhang, M., et al. (2016). Removal of phosphate from aqueous solutions using biochar-supported nanoscale zero-valent iron. Water Research, 92, 63-71. https://doi.org/10.1016/j.watres.2016.01.033

[72] Liu, Y., et al. (2018). Enhanced removal of phosphate using nanoscale zero-valent iron modified by silver nanoparticles. Journal of Hazardous Materials, 346, 217-226. https://doi.org/10.1016/j.jhazmat.2017.12.038

[73] Wu, D., et al. (2020). Stabilization of nanoscale zero-valent iron by green synthesis and its application in environmental remediation. Environmental Science & Technology, 54(10), 6357-6367. https://doi.org/10.1021/acs.est.9b07645

[74] Qu, X., et al. (2013). Nanotechnology for a safe and sustainable water supply: Enabling integrated water treatment and reuse. Accounts of Chemical Research, 46(3), 834-843. https://doi.org/10.1021/ar300194w

[75] Zhang, W., Liu, Y., Li, J., Yu, H., & Chen, Y. (2020). Synergistic effects of nanoscale zero-valent iron and silver nanoparticles for enhanced contaminant removal: Role of electron transfer and reactive species generation. Journal of Hazardous Materials, 384, 121429. https://doi.org/10.1016/j.jhazmat.2019.121429

[76] Rai, M., Yadav, A., & Gade, A. (2012). Silver nanoparticles as a new generation of antimicrobials. Critical Reviews in Microbiology, 38(4), 313-331. https://doi.org/10.3109/1040841X.2011.623477

[77] Liu, Y., Li, T., Yang, L., & Zhang, L. (2018). Enhanced phosphate removal by nanoscale zero-valent iron supported on biochar: Role of Ag doping and mechanisms. Water Research, 137, 120-129. https://doi.org/10.1016/j.watres.2018.03.006

[78] Jha, A. K., Prasad, K., & Kulkarni, A. R., (2009). Plant System: Natures Nanofactory. Colloids and Surface Biointerfaces, 73, 219-223.